Hindawi
Structural Control and Health Monitoring
Volume 2024, Article ID 6662678, 19 pages
https://doi.org/10.1155/2024/6662678

Research Article

A New Method for the Compaction Quality Inspection of High Rockfill Dams Based on 3D Laser Scanning Technology

Qiang Yao,[1,2] Yu Wu,[3] Jun He,[4] Shunchao Qi,[1] and Hongtao Li[1]

[1]*State Key Laboratory of Hydraulics and Mountain River Engineering, College of Water Resource and Hydropower, Sichuan University, Chengdu, Sichuan 610065, China*
[2]*Technology Innovation Center for Risk Prevention and Mitigation of Geohazard, Ministry of Natural Resources, Chengdu, Sichuan 611734, China*
[3]*Chengdu Engineering Corporation Limited, Chengdu, Sichuan 610072, China*
[4]*Sinohydro Bureau 7 Co., Ltd., Chengdu, Sichuan 610213, China*

Correspondence should be addressed to Hongtao Li; htl@scu.edu.cn

Received 21 August 2023; Revised 26 December 2023; Accepted 11 January 2024; Published 3 February 2024

Academic Editor: Francesc Pozo

The compaction quality is directly related to the deformation and stability of the rockfill dam. Measuring the test pit volume efficiently and accurately is the most critical step during the compaction quality inspection. A new method for calculating the test pit volume based on point cloud data is proposed. An auxiliary device that can change the scanning distance and angle of the handheld 3D laser scanner is developed to collect the initial point cloud. The segmentation method of the initial point cloud data including the test pit and the compaction surface outside the pit is to divide the data into two parts according to the order number of the segmentation point, after slicing and sorting point clouds, which is the key to ensuring the computational precision. The segmentation points are the adjacent two points with the greatest order number difference in these point clouds whose distance from the line connecting the end points of the slicing point clouds is less than d_z. The compaction surface point clouds are used to construct a plane by the least-squares algorithm so that the closed three-dimensional model is formed by registering it with the test pit point clouds. After converting the test pit surface to the horizontal plane by the Rodrigues formula, the test pit point clouds are divided into n^2 parts with equal projection areas on the horizontal plane, and n^2 prisms are constructed using them and their projection areas. The test pit volume is the sum of the intersection space volumes of all prisms and the test pit model, and the intersection space is determined by comparing the Z-values of point clouds. The new method was programmed in MATLAB and applied to the Shuangjiangkou rockfill dam with a height of 315 m. The relative error of volume results between the new method and the old water-filling method is 0.14–2.31%. The cause of the error is analyzed, and it is proved that the results of the new method are closer to the real volume of the test pit in theory. This method reduces the inspection cost but greatly improves the level of precision, efficiency, and intelligence for compaction quality inspection.

1. Introduction

The rockfill dam plays an important role in achieving the carbon peak and carbon neutrality target with its comprehensive advantages, such as local materials, good seismic resistance, and a low carbon footprint [1–4]. A series of high rockfill dams with a height of more than 300 meters will be developed in Gushui, Ri Coronation, and Qizong, China. The quality of compaction construction is a key factor in ensuring the safe and stable operation of dam projects, which is directly related to the overall settlement deformation and stability of the dam body [5–7]. High rockfill dams place higher demands on compaction quality [8, 9].

According to the *Specification for Rolled Earth-rockfill Dam Construction DT/L 5219-2013*, the "double control" method, which combines the rolling control parameters (the thickness of paved materials and rolling times) with the postrolling sampling pit parameters (compactness, etc.), is used to manage the compaction quality of rockfill dams [10]. In the field construction of compaction quality testing, the

test pit volume is measured by a human water-filling method [11]. However, the traditional method's measurement results are susceptible to the human factor, making them not only unreliable and low in precision but also time-consuming and inefficient [12]. In severe cases, even substandard compaction quality is mistaken for a pass, resulting in a shorter lifetime of the dam [13]. Therefore, there is an urgent need for a test pit volume measurement method with greater accuracy, efficiency, and stability.

3D laser technology is becoming an important tool for precision measurement and testing with its advantages of rapidly scanning the surface of the measured object and directly obtaining high-resolution point cloud data [14–18]. Sedek and Serwa [19] developed a semiautomatic approach for forming and processing laser sensing data of trusses using ANN. Serwa and Saleh [20] developed a software applying neural network and proposed a semiautomatic three-dimensional registration method for laser scanning data of bridge structure ground. Ahmed Nabil et al. [21] developed the microanalysis of the bituminous mixtures using the 2D scanner and image analysis techniques (IAT). Sedek and Serwa [22] applied laser remote sensing data of an as-built model, with BrlM (bridge information model) for a constructed bridge. Many researchers have successfully applied 3D laser technology to the water engineering industry, thus significantly improving work efficiency and data accuracy in areas such as dam deformation monitoring, reservoir volume measurement, and dam crack identification [23–25]. 3D laser technology is currently the most effective means to acquire information on irregular object shapes, sizes, areas, and volumes. Numerous studies have verified the accuracy of volume measurement of irregular objects using 3D laser technology [26–35]. For the volume calculation of irregular objects, the usual method is to slice the point cloud model and then calculate the volume of each layer separately before summing it up or to fit the point cloud model to a geometric model where the volume can be easily calculated. For example, Huang [26] divided tree stem point clouds into vertical layers and estimated the total volume by calculating the volume of each layer. Some researchers proposed estimating the volume of tree stems by modelling them as cylinders, considering their shapes [26–28]. Shao et al. [31] adaptively determined the optimal point-reducing intervals of scanning lines by PSO and obtained higher volume estimation accuracy compared with the average distance method. Cai et al. [32] repaired the point clouds by interpolating points and completed the calculation of potato volume by establishing a cylindrical coordinate system. Wang et al. [33] estimated the total volume of wheat spikes by fitting their shapes with small cubes generated by the adaptive k-means algorithm. More academics are optimizing the preprocessing of point cloud data to produce more accurate models in order to increase the precision and speed of volumetric measurements. Guevara et al. [34] proposed an improved α-shape algorithm to estimate the layered volume more accurately. Chi et al. [36] presented an end-to-end method that addresses the existing limitation by hybridizing augmented reality (AR) and laser scanning technologies to provide intuitive and accurate rebar inspection. Chéruel and Ftima [37] presented a critical review of experimental methods to assess the unrestrained ASR volumetric expansion and discuss the influence of size and aspect ratio effects on its anisotropy. Volumetric expansions were assessed using a conventional method (DEMEC strain gauge and an outside micrometer) and a new innovative method using 3D-handled laser scanning technology. Numerous studies have offered ideas for measuring the volume of highly irregular test pits. However, the above volume calculation methods are all based on the target point cloud model, but the compaction surface outside the test pit will inevitably be scanned during the point cloud acquisition process. How to effectively extract the test pit model from this type of data, where the target point clouds and redundant point clouds are connected, is critical to ensuring volume accuracy. In addition, the test pit is not enclosed, so its surface needs to be modeled so that the volume information can be further obtained.

In response to the aforementioned issues, this paper adopts the slicing-segmenting method to divide the data into compaction surface point clouds and test pit point clouds, further fitting the test pit surface based on the compaction surface point clouds.

2. Method

2.1. Point Cloud Data Collection. Data such as geometric dimensions and structural features are hidden in 3D point clouds. The accuracy of information extraction is first determined by the quality of the point cloud. High-quality data can reduce measurement errors when applying the 3D laser to the dam compaction quality inspection. However, the test pit, used for quality sampling, is extremely irregular in shape. Whose concave and convex walls block the path of the laser, resulting in a large blind area. To guarantee the quality of the point cloud that is captured, a 3D laser scanner that is appropriate for the test pit must be chosen.

2.1.1. Test Pit and Scanning Device. In Figure 1(a), the construction material of the rockfill dam generally consists of the core material, the filter material, the transition rockfill, and the rockfill. A large number of pores that are filled with water and air exist in each type of material, which must be compacted by rolling back and forth through machinery. Only if the compaction quantity meets requirements, the next layer can be paved. For compaction inspection, it is usually obtained through the test pit method. The method requires that the diameter of the test pit should not be less than 2-3 times the maximum particle size of the dam material, but the maximum should not exceed 2 m. The depth of the test pit should be the thickness of the paved layer. For various types of dam materials, due to their different particle size distribution, the size of the test pits is also different. The pit diameter of core material (Figure 1(I)) and filter material (Figure 1(II)) is about 0.3 m, while that of the transition rockfill (Figure 1(III)) is approximately 1 m and roughly 2 m for rockfill (Figure 1(b-2)).

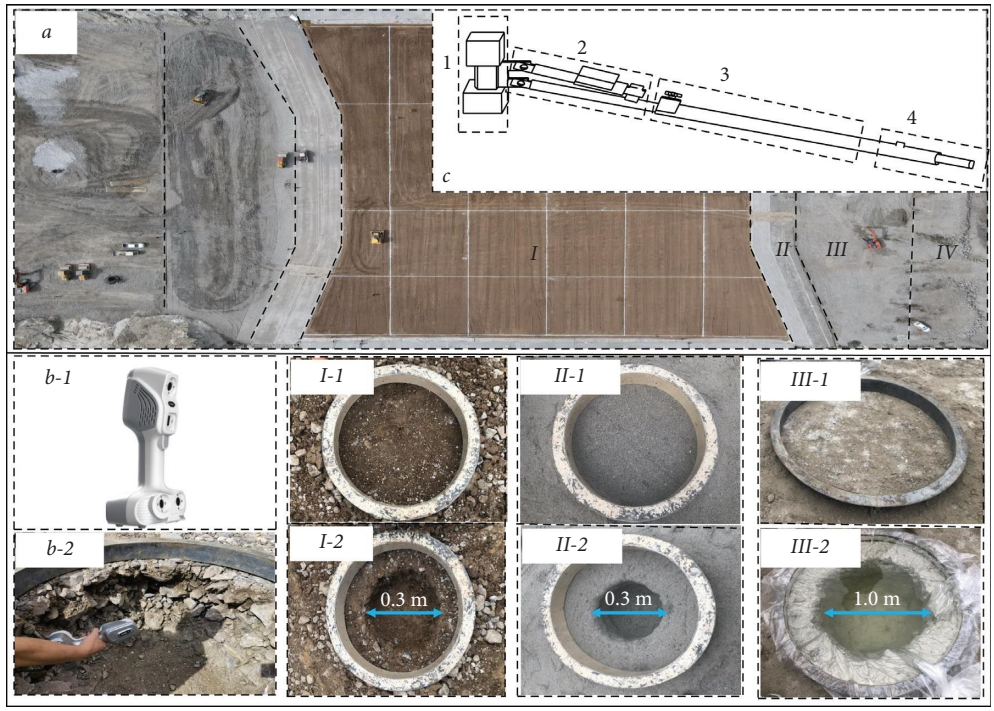

Figure 1: Test method for the compaction quality of rockfill dams.

In Figure 1(a), the rockfill dam generally consists of the core material (I), the filter material (II), the transition rockfill (III), and the rockfill (IV). Each type of material contains a large number of pores that are filled with water and air, which must be squeezed out during the rolling process. After the rolling, the material can be paved and filled again only after the test parameters have been qualified. The degree of compaction is the key test index, often using the pit sampling method. The method requires that the pit depth be basically the same as the paving thickness; the pit diameter shall be 3 times the maximum particle size of the material, but its maximum diameter should not exceed 2 m. The paving thickness and the maximum particle size are different for each type of dam material, so the sampling pit method requires different pit sizes. The pit diameter of filter material and core material is about 0.3 m (Figures 1(I-2) and 1(II-2)), while that of the rockfill is approximately 2 m and roughly 1 m for transition rockfill (Figure 1(III-2)).

The handheld 3D laser scanner (Figure 1(b-1)) is small and used flexibly, so it can be held to reach inside the pit for data collection, reducing the blind spot in the scanning process (Figure 1(b-2)). Based on IREAL 2S, the surface shape of the test pit is not damaged during the data collection process, and the nondestructive acquisition of the point cloud is achieved. Its basic scanning parameters are shown in Table 1. However, the maximum optimal scanning distance of IREAL 2S is 650 mm, so when applied to data collection of large-sized inspection pits, there may be a problem of short scanning distance, which makes it difficult to effectively collect point clouds in the bottom area of the inspection pit.

Also, this equipment can collect all the data at once, making it a suitable device for the acquisition of pit point clouds. However, when used in large pits, the scanning distance of the handheld scanner is so short that the point clouds at the bottom of the pit cannot be collected. In this paper, an auxiliary device with variable scanning distance and angle has been developed and is used in conjunction with a handheld scanner, as shown in Figure 1(c). The handheld 3D laser scanner (1) is mounted on the head of the auxiliary device. The pole body (3) is telescopic, so the scanning distance can be increased or decreased by changing the length of the pole, aiming to suit different pit sizes. The orientation of the scanner is controlled by the rotating pusher (2), so the scanning angle can be changed at any time by controlling the controller, whose power (4) is fixed at the end of the pole. This assistive device overcomes the shortcomings of the handheld scanner yet retains its flexible scanning characteristics.

2.1.2. Data Collection. Before using a scanner for work, appropriate scanning parameters are first set based on the size of the test pit, mainly including scanning accuracy, light source, and registration mode. In general, the relevant parameter settings can refer to Table 2.

After the parameter settings are completed, the data collection process for the test pit point cloud is as follows: first, scan the surface area of the pit wall on the top layer of the test pit (Figure 2(a)), including the dam material surface area with a certain width around the pit wall, to ensure the integrity of the test pit point cloud data and then slowly

Table 1: Basic parameters for IReal 2S.

Type		IREAL 2S	
Light source	Type	Blue	Red
	Visibility	Yes	No
	Safety	Eye safe	Eye safe
Scan accuracy	Point spacing	~0.1 mm	~0.15 mm
	Registration	~0.2 mm/m	~0.25 mm/m
Registration mode	No maker	Texture, feature, and blending	
	Marker	Marker and blending	
Scan range	Optimal scanning distance	350–650 mm	
	Effective working distance	250–1000 mm	
	Maximum scanning area	520 ∗ 510 mm	
Speed	Maximum scanning speed	1500000 points/second	
Hardware	Weight	910 g	
	Size	140 ∗ 94 ∗ 258 mm	

Table 2: Parameter settings for point cloud collection in test pits.

	Point spacing (mm)	Light source	Registration mode
Core material/filter material	~1	Blue	Feature
Transition rockfill	~2	Blue	Feature
Rockfill	~3	Red	Feature

increase the scanning distance, gradually transitioning from the top layer of the pit wall area to the bottom layer of the pit wall area by increasing the length of the telescopic rod (Figure 2(b)). For the collection of point cloud data in the bottom area of the detection pit, the scanning direction is controlled in real time using an electric push rod (Figure 2(c)). When there are pits or protrusions in the scanning area, the scanner head should be pushed by a push rod to turn, causing real-time changes in the scanning angle, thus achieving all-round and efficient collection in the concave and convex areas (Figure 2(d)). By using the above operation methods, high-quality and complete detection pit point cloud data can be collected, providing strong data support for subsequent measurement of compaction quality.

2.2. Data Processing. It is inevitable to scan the dam material surface area outside the target area during the data collection process. However, these excess data will increase the error, so it is necessary to remove the extra part in order to obtain the target point cloud. Besides, the excavation surface in the sampling area needs to be modeled and concatenated with the segmented point cloud data to form a closed three-dimensional test pit model.

In the compaction construction of filling dam materials, the dam material surface is required to be compacted and leveled. During the compaction quality inspection, a secondary leveling treatment is also performed on the dam material surface in the sampling area (Figure 1). Therefore, the dam material surface in the sampling area can be approximated as a plane. The point cloud of the dam material surface outside the test pit can be used as the reference for fitting the excavation surface of the test pit. The point cloud processing process is shown in Figure 3.

The segmented dam material surface point cloud should not include the pit wall area, to prevent excessive pit wall area point clouds from causing significant deviation in the fitting plane. This paper proposes a segmenting method by slicing the point cloud data. This method is based on the correctly sorted section point cloud, and precise control of segmentation position is achieved by adjusting the sorting numbers of split points.

2.2.1. Point Cloud Slicing. The commonly used point cloud slicing is the projection method. The principle is to first choose point clouds in the layered area and then project them onto a plane [38–40]. For the segmentation of the section point cloud, the point cloud within the layered region needs to be acquired without further processing them. The slicing thickness is typically twice the point cloud spacing, with the goal of ensuring the contour integrity of the slicing point clouds while also preventing a large slicing thickness from affecting the subsequent point cloud processing. The section point cloud is shown in Figure 4 after the data are sliced along the X-axis.

2.2.2. Point Cloud Sorting. In order to realize the accurate segmentation of the section point cloud, this paper proposes a method based on extracting the split points. However, the point cloud data collected by the 3D laser scanner are disordered and often cannot be applied directly to data processing, so it is necessary to use a suitable sorting method to arrange a bunch of scattered point clouds in a specific order. The sorted point clouds will significantly improve the efficiency and correctness of point cloud processing. As the slicing thickness is twice the point cloud spacing, point cloud

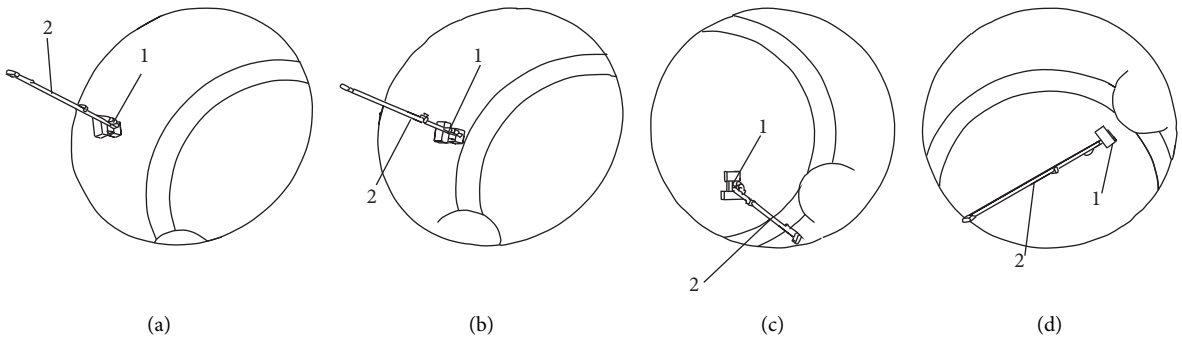

Figure 2: Schematic diagram of the process for collecting point clouds (where 1 is the handheld scanner and 2 is the auxiliary device).

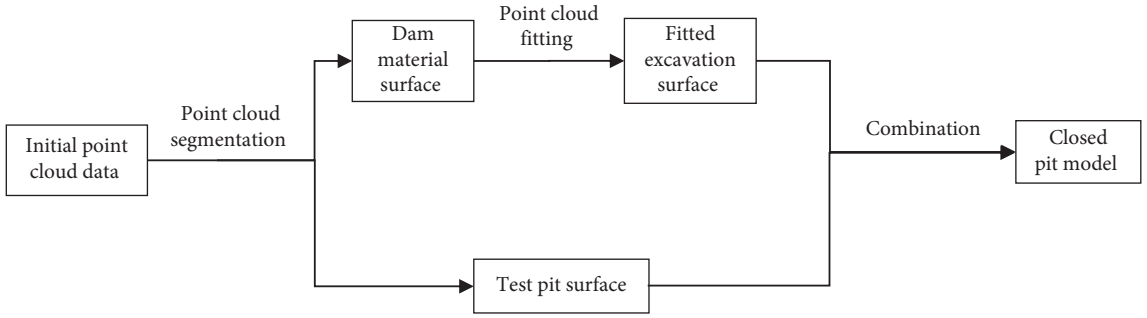

Figure 3: Flowchart for point cloud processing.

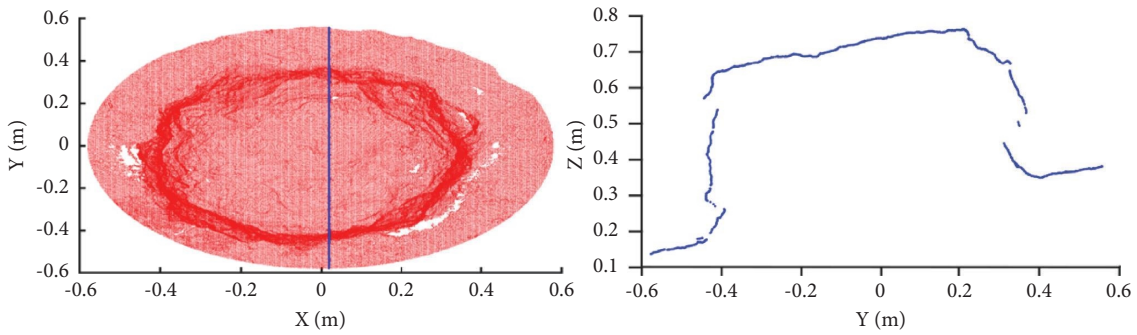

Figure 4: The section point cloud is sliced along the X-axis.

bands are bound to exist at certain locations. The sorting method as follows is used to achieve correct sorting of section point cloud.

As shown in Figure 5, based on the point clouds layered along the X-axis, we select the point cloud segment inside the radius r of point a_1 with the smallest Y-value and rotate it using the rotation matrix R_1 so that the segment's endpoint line (a_1a_n) is parallel to the Y-axis. The segment is then sorted according to its Y-value $(a_1 \ldots a_n)$. Next, we select the point cloud segment with the radius range r of b_1 (the nearest point of a_n), and we repeat the sort method described above to obtain the sorting result $(b_1 \ldots b_n)$. We recombine two sorting results $(a_1 \ldots a_n$ and $b_1 \ldots b_n)$. We select the other point cloud segments in turn until the entire slicing point clouds are sorted. So, the correct sorting is achieved, as shown in Figure 6.

Rotation matrix R_1 is as follows:

$$R_1 = \begin{bmatrix} 1 & 0 & 0 \\ 0 & \cos\beta & -\sin\beta \\ 0 & \sin\beta & \cos\beta \end{bmatrix}. \quad (1)$$

2.2.3. Point Cloud Segmenting. Due to the high flatness of the dam material surface, it is easy to select a spatial area containing the dam material surface point cloud in the slice point cloud. In Figure 7, for the point cloud sliced along the X-axis, the line connecting the endpoints (n_1, n_n) is shifted to a position that coincides with the Y-axis by rotation and translation. The rotation method is the same as the point cloud sorting mentioned above. Point cloud segmentation is

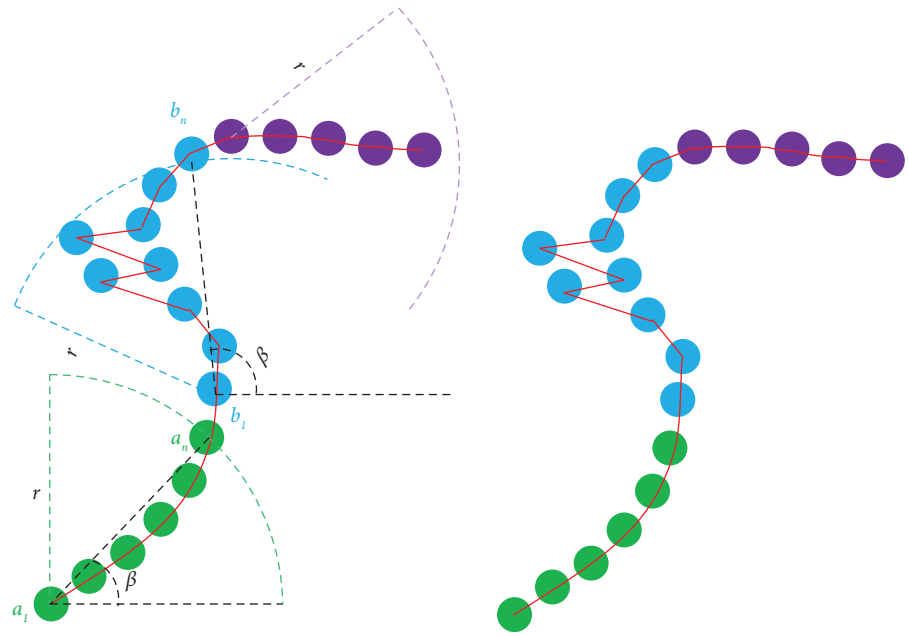

FIGURE 5: Schematic diagram of sorting method for the section point cloud (β is the included angle between the segment's endpoint line and the Y-axis).

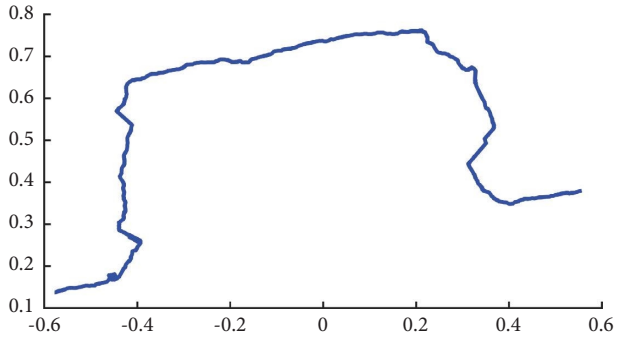

FIGURE 6: The sorting result for the section point cloud.

achieved by setting a height threshold. When the threshold is large enough, such as z_1, all point clouds on the dam material surface can always be selected, but this results in multiple point clouds belonging to the surface of the test pit, as shown in Figure 7(a). When the threshold is small, such as z_2, it will cause some dam material surface point clouds to be missed, as shown in Figure 7(b).

In order to solve the problem of incorrect or missed selection, this paper uses the sorted section point cloud to cluster and segment based on the segmentation point number. The steps of the method are as follows: first, we select the point cloud collection in the section point cloud where the Z-value is less than z_2, and we extract the two adjacent points (n_a, n_b) that have the highest difference in sorting numbers. n_a and n_b are the two segmentation points. By comparing the size of the sorting number of the section point cloud and segmentation point number, the dam material surface point cloud and the test pit surface point cloud are determined. That is, points with sorting numbers less than n_a and greater than n_b are clustered as dam material surface point cloud, and points with sorting numbers between n_a and n_b are clustered as test pit surface point cloud. This method can effectively solve the problem of missing point cloud selection on the dam material surface, as shown in Figure 8. However, due to the segmentation points n_a and n_b being located in the pit wall area of the test pit, it still leads to the selection of more pit wall point clouds for the segmented dam material surface point cloud, while the segmented test pit surface point cloud may lack some pit wall point clouds.

In order to better meet the segmentation requirements, based on the segmentation points n_a and n_b, the selection of point clouds on the dam material surface and the test pit surface can be controlled by adjusting the sorting number of the segmentation points. As shown in Figure 9, for the point cloud of the dam material surface, two points with sorting numbers n_a/N and $n_b + (n_n - n_b)/N$ are selected as the segmentation points of the dam material surface point cloud, and points with sorting numbers between $n_b + (n_n - n_b)/N$ and n_a/N are selected as the dam material surface point cloud. The above processing is equivalent to only taking the $1/N$ ($N \geq 1$) part of the area between the segmentation point and the outermost point of the dam material surface, thereby avoiding errors in selecting the test pit point cloud and causing deviations in the fitting plane. For the point cloud on the surface of the test pit, we select two points with sorting numbers $n_a - n_d$ and $n_b + n_d$ as the segmentation points of the point cloud on the surface of the test pit, and we use point clouds with sorting numbers less than $n_a - n_d$ and greater than $n_b + n_d$ as the point cloud on the surface of the test pit. n_d is the number of point clouds included in the difference in Z-value distance between the segmentation point and the average coordinates of the point cloud on the dam material surface for the same point spacing. Increasing

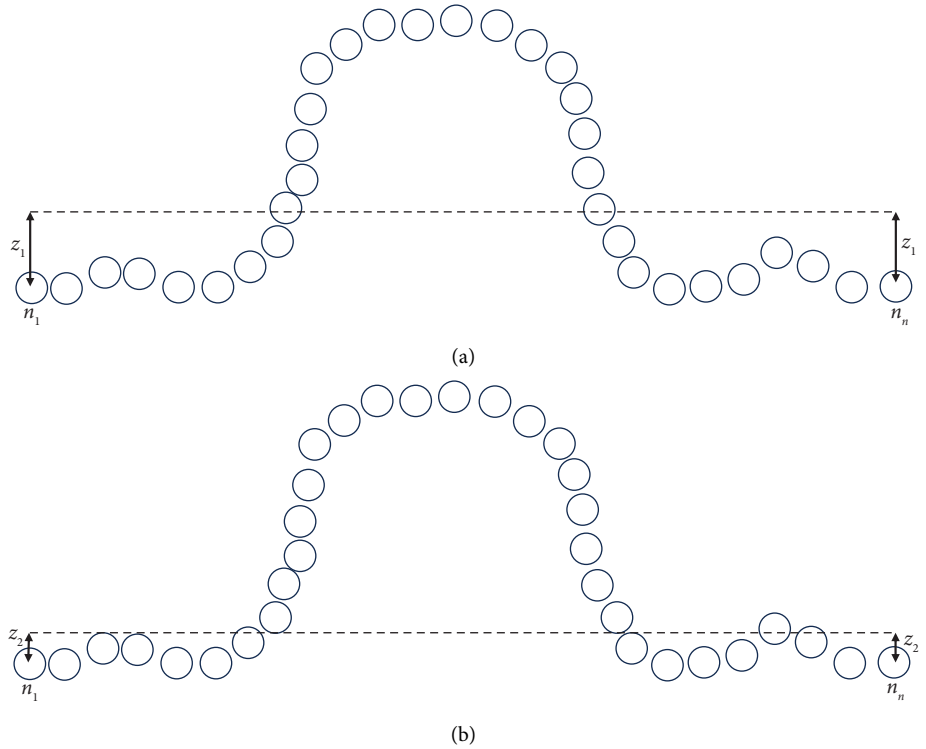

FIGURE 7: Selection of point clouds on dam material surface. (a) The height threshold is z_1. (b) The height threshold is z_2.

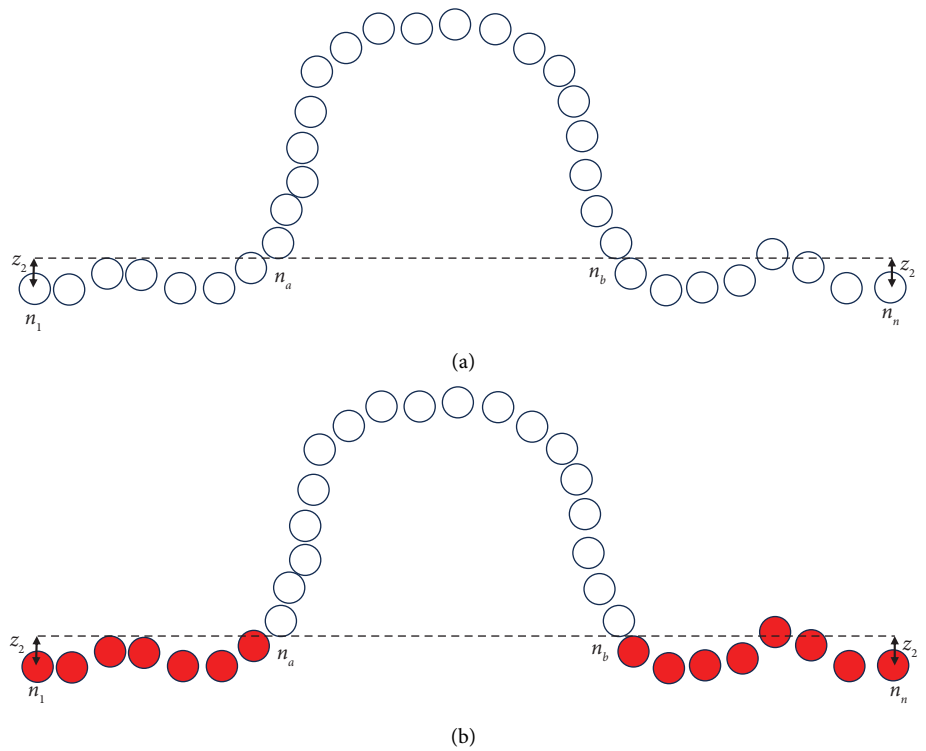

FIGURE 8: Selection of point clouds on dam material surface. (a) Segmentation points n_a and n_b. (b) Schematic diagram of segmentation results.

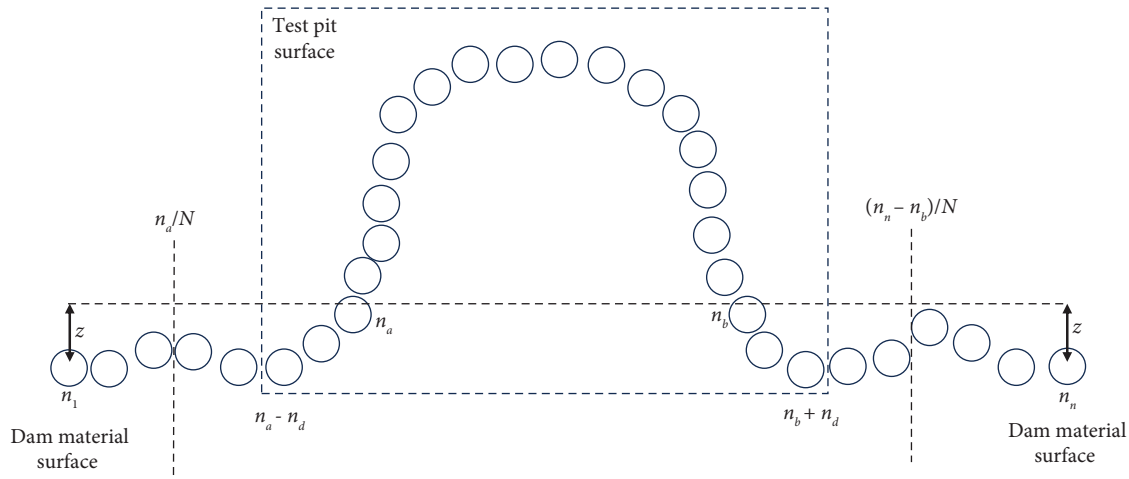

Figure 9: Schematic diagram of segmentation method for slicing point clouds.

the number of point clouds with n_d is to ensure the integrity of the test pit point cloud. The segmentation effect is shown in Figure 10.

2.2.4. Point Cloud Filling. Although the method and device for data acquisition described in this paper have minimized the blind area during scanning, there are still some holes in some corner areas of the pit wall. The findings of the pit volume calculation will be affected if the holes are not filled. For sorted section point clouds, it is easy to repair pit wall point clouds through linear interpolation. The specific method is as follows: based on the correctly sorted section point cloud, we select two adjacent points in the test pit point cloud in the order of the point cloud sorting number. If the Euclidean distance between the two points is greater than the point spacing, we interpolate them, as shown in Figure 11(a). Through this method, the contour of the section point cloud can be quickly repaired. Due to the small diameter of the holes, the linear filling method will not cause significant deviation between the test pit model and the actual test pit. Figure 11(b) shows the effect of section point cloud filling.

2.2.5. Compaction Surface Point Clouds and Test Pit Point Clouds. Based on the above method, the point clouds in the middle region of the data can already be segmented precisely while the holes of the test pit are repaired. However, when the slicing position is in the edge wall area of the test pit, the obtained section point cloud contours are interlaced with each other, as shown in Figure 12. Continuing to use the above sorting method will result in incorrect sorting, resulting in incorrect segmentation and filling. In order to achieve accurate segmentation of the section point cloud in the edge wall area, the point cloud data can be rotated at a certain angle to convert it to the middle area of the test pit. Continuing to use the segmentation method can obtain the correct segmentation results of the point cloud data in the edge wall area.

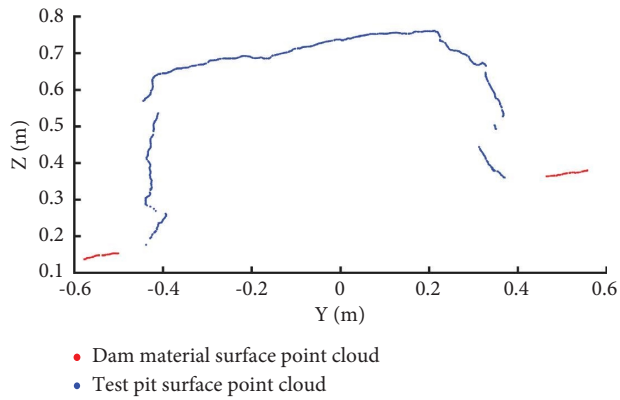

Figure 10: The segmentation effect for slicing point clouds ($N = 2$).

For the complete segmentation of test pit point cloud data, we first slice and segment the point cloud in the middle of the data. Then, the point cloud data originally located in the edge wall area are rotated to a certain angle to convert it to the middle area of the test pit, and the point cloud data in the middle part are segmented again. We repeat the above steps until the dam material surface and the test pit surface are obtained. The segmentation effect is shown in Figure 13.

2.2.6. Reconstruction of Test Pit Model. By adjusting the position of the segmentation points, it is effectively ensured that the point cloud of the segmented dam material surface does not include the pit wall area. Before the excavation of the test pit, the area of the dam material surface is approximately flat, so the least squares method can be used to fit the point cloud of the dam material surface in a plane, and the fitting plane can be used as the sampling area of the dam material surface.

The fitting plane expression is as follows:

$$z = a_0 * x + a_1 * y + a_2. \quad (2)$$

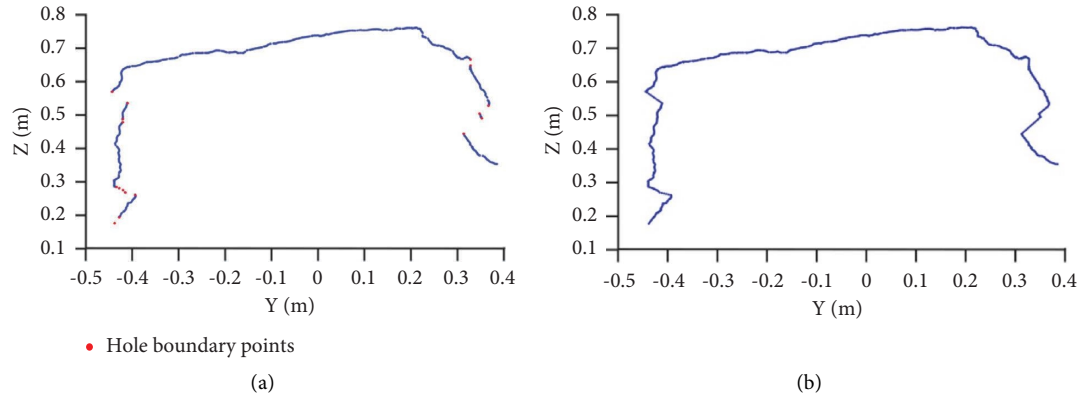

Figure 11: Linear filling method for section point clouds. (a) Selection of hole boundary points. (b) Hole filling effect.

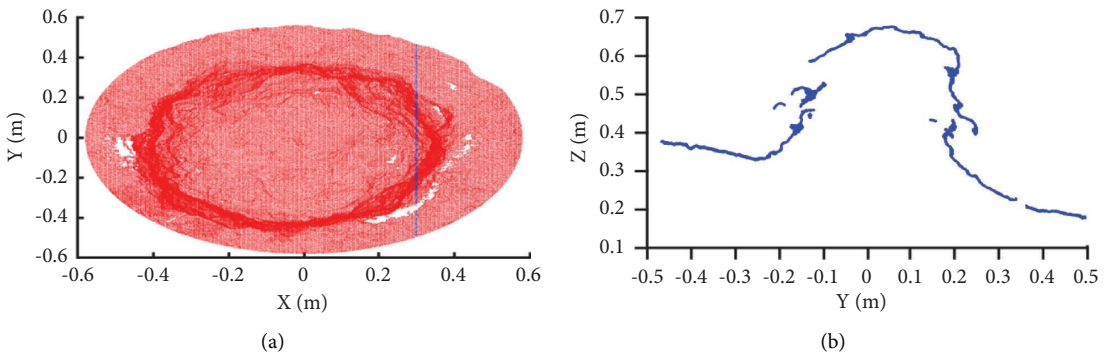

Figure 12: Section point cloud in the pit sidewall area.

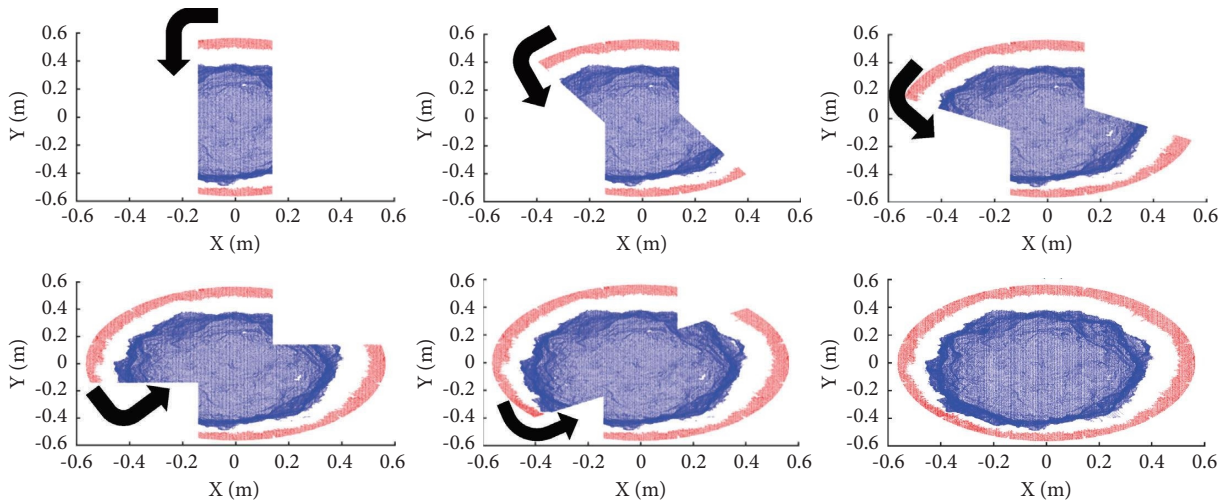

Figure 13: The segmenting processes of the whole point clouds (the rotation angle is 30° and the time of rotation is 6).

According to the principle of least squares, the fitting plane should meet the minimum error sum of squares, which means that the following conditions are met.

$$\begin{cases} \sum_{i=0}^{n-1} 2\left(a_0 x_i + a_1 y_i + a_2 - z_i\right) \cdot x_i = 0, \\ \sum_{i=0}^{n-1} 2\left(a_0 x_i + a_1 y_i + a_2 - z_i\right) \cdot y_i = 0, \\ \sum_{i=0}^{n-1} 2\left(a_0 x_i + a_1 y_i + a_2 - z_i\right) = 0. \end{cases} \tag{3}$$

The matrix form is as follows:

$$\begin{bmatrix} \sum_{i=0}^{n-1} x_i^2 & \sum_{i=0}^{n-1} x_i y_i & \sum_{i=0}^{n-1} x_i \\ \sum_{i=0}^{n-1} x_i y_i & \sum_{i=0}^{n-1} y_i^2 & \sum_{i=0}^{n-1} y_i \\ \sum_{i=0}^{n-1} x_i & \sum_{i=0}^{n-1} y_i z_i & n \end{bmatrix} \begin{bmatrix} a_0 \\ a_1 \\ a_2 \end{bmatrix} = \begin{bmatrix} \sum_{i=0}^{n-1} x_i z_i \\ \sum_{i=0}^{n-1} y_i z_i \\ \sum_{i=0}^{n-1} z_i \end{bmatrix}, \tag{4}$$

where x_i, y_i, and z_i are the position coordinates of each point in the point cloud data of the dam material surface.

By solving the matrix, the coefficients a_0, a_1, and a_2 are obtained. The normal vector of the fitting plane for the point cloud data of the dam material surface is (a_0, a_1, −1), and then, the Euclidean distance d_0 between the fitting plane and the coordinate origin is as follows:

$$d_0 = \frac{|a_2|}{\sqrt{1 + a_0^2 + a_1^2}}. \tag{5}$$

The point cloud fitting plane of the dam material surface is concatenated with the point cloud of the test pit surface to form a closed model, thus achieving the reconstruction of the three-dimensional model of the test pit, as shown in Figure 14.

2.2.7. Rodrigues Formula. Due to the unfixed spatial position of the test pit model (Figure 15(a)), directly calculating the volume will increase complexity, and it is difficult to consider reducing the impact of concave and convex pit walls on the volume calculation results. Therefore, the fitting plane of the test pit model can be rotated parallel to the coordinate plane XOY (Figure 15(c)). The normal vector of the fitting plane is normalized to $\vec{n_0}$, and the distance between the fitting plane and the coordinate origin is d_0. According to the *Rodrigues* formula, the fitting plane normal vector is rotated by a certain angle θ around the rotation axis (k_x, k_y, k_z), while $\vec{n_0}$ convert it to $\vec{n_1}$ (0, 0, 1) (Figure 15(b)), and the rotation matrix of the conversion process is R_2.

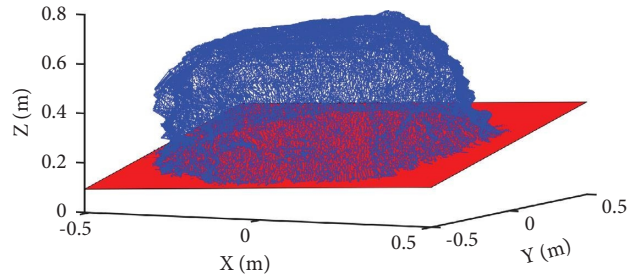

Figure 14: 3D model of the closed test pit.

In Figure 15(b),

$$\begin{aligned} \vec{k} &= \vec{n_0} \times \vec{n_1}, \\ \vec{n_1} &= R_2 \cdot \vec{n_0}, \\ R_k &= \begin{bmatrix} 0 & -k_z & k_y \\ k_z & 0 & k_x \\ k_y & k_x & 0 \end{bmatrix}, \\ R_2 &= I + \sin(\theta) \cdot R_k + (1 - \cos\theta) \cdot R_k^2. \end{aligned} \tag{6}$$

According to the rotation matrix R_2, we rotate the point cloud on the surface of the test pit and convert its displacement distance d_0 to the position as shown in Figure 15(c). At this time, the fitting plane of the test pit model is converted into the coordinate plane XOY.

2.2.8. Volume Calculation. Volume calculation based on point cloud data generally involves layering the model and then summing the volumes of each layer. The essence of the method is to simplify the three-dimensional surface reconstruction problem to a two-dimensional curve reconstruction problem, but it requires generating boundary polygons for the section contour. The two-dimensional computational problem can be further simplified into a one-dimensional problem. After converting the fitting plane of the test pit model into the coordinate plane XOY, the volume of the test pit can be calculated by projecting the point cloud on the surface of the test pit onto the coordinate plane XOY. The projected area is divided into n^2 tiny regions, each of which has an area of $\Delta x_i * \Delta y_i$, and is formed into a small prism with the point cloud of the test pit surface projected within the $\Delta x_i * \Delta y_i$ region. The sum of the intersection space volumes of all the prisms and the test pit model is the volume of the test pit, as shown in Figure 16. The volume of intersection space is $\Delta x_i * \Delta y_i * h$, where h is the length of the intersection space.

Due to the uneven shape of the test pit wall, there are always multiple point clouds projected onto the same area, which can affect the results in the volume measurement of the test pit. In nonpit wall areas, only one point cloud is projected onto the same area, while in pit wall areas, multiple

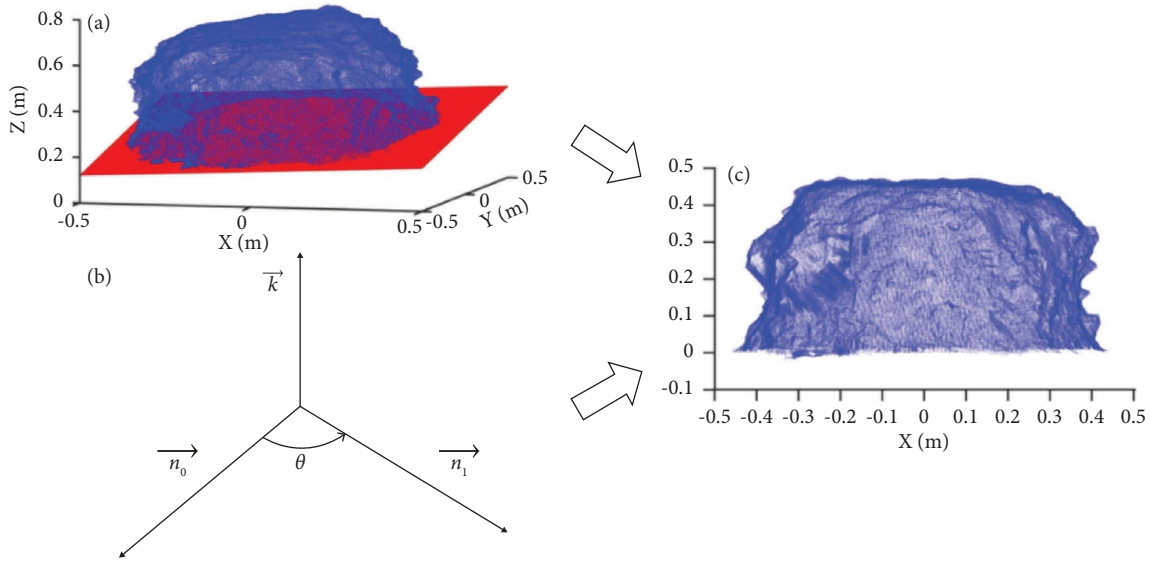

Figure 15: Rotating the point clouds based on *Rodrigues* formula: (a) 3D model of closed test pit; (b) schematic diagram of *Rodrigues* formula; (c) test pit point clouds after converting its surface to the XOY plane.

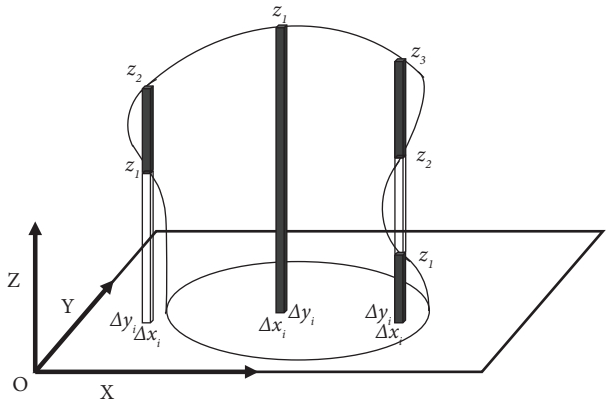

Figure 16: Schematic diagram of intersecting space volume calculation.

point clouds are projected onto the same area. Therefore, in small prisms, the distribution of point clouds can be used to identify the concave and convex areas of the pit wall, in order to reduce the impact of concave and convex pit walls on the volume measurement results of the test pit. When calculating the length h of the intersecting space, the points inside the small prism are arranged in descending order of z-coordinate values. If the difference in coordinates between adjacent two points at m is greater, it is considered that there is a point cloud with interval distribution at m within the small prism.

The length h of its intersection area is as follows:

$$h = z_m\text{-}z_{m\text{-}1} + z_{m\text{-}2} + \cdots + (-1)^{(m+1)} z_1. \tag{7}$$

Total pit volume V is as follows:

$$V = \sum_{i=1}^{n} \Delta x_i \Delta y_i h_i, \tag{8}$$

where z_i is the average value of the z-coordinate values of each point cloud.

2.3. Compaction Quality Index. Combining relevant algorithms in the calculation of test pit volume, a compaction quality inspection program was written using MATLAB as the programming platform. According to the Specification for Rolled Earth-rockfill Dam Construction DT/L 5219-2013, the quality index of different dam materials varies, such as using compaction ratio for core wall materials, relative density for filter materials, and porosity for transition materials and rockfill materials. The compaction ratio of the entire material is the ratio of dry density to maximum dry density, where the maximum dry density $\rho_{\max}$ is the dry density corresponding to the peak point on the relationship curve between dry density and moisture content obtained from the compaction test, and the dry density ρ_d is as follows:

$$\rho_d = \frac{m}{(1+w)\cdot V}, \tag{9}$$

where V is the volume of the test pit, m is the mass of the dam material, and w is the moisture content.

The relative density d is as follows:

$$d = \frac{\rho_{\max}\cdot(\rho_d - \rho_{\min})}{\rho_d\cdot(\rho_{\max} - \rho_{\min})}, \tag{10}$$

where $\rho_{\min}$ is the minimum dry density.

The porosity n is as follows:

$$n = \frac{1-\rho_s}{\rho_d}\cdot 100, \tag{11}$$

where ρ_s is the particle density of the dam material.

It can be seen that these quality indexes need to be further calculated by measuring the volume of the test pit, and the volume is extracted from the point cloud data of the test pit using the volume calculation method proposed in this paper. Other parameters such as weight are obtained through on-site weighing, and moisture content is obtained through experiments.

3. Engineering Application

3.1. Shuangjiangkou Rockfill Dam. Shuangjiangkou hydropower station is located in Maerkang County and Jinchuan County, Sichuan Province, and is the upstream reservoir project of hydropower gradient development in the Dadu River Basin. The development mission of the power station is mainly to generate electricity, adopting the dam type of development. The normal storage level of the reservoir is 2500 m, with a total capacity of 2.897 billion m^3 and 1.917 billion m^3 for a regulating capacity. In Figure 17, the water-retaining structure is a gravel soil core wall rockfill dam, with a maximum height of 315 m, a top width of 16.0 m, and a dam crest length of 639 m. The dam's crest elevation is 2510 m, and the bottom elevation of the gravel soil at the riverbed is 2195 m. The slope ratio of the upstream dam is 1 : 2.0 and 1 : 1.9 for the downstream dam slope ratio. The water-retaining dam body is divided into four major zones: the impermeable body, the filter layer, the transition layer, and the dam shell. The impermeable body adopts the type of gravel soil core wall, and the dam shell is filled with rockfill. A filter layer and a transition layer are provided between the impermeable body and the upstream and downstream dam shells. For the impermeable body, the top width is 4 m, and the upstream and downstream slopes are both 1 : 0.2, while the top and bottom elevations of the impermeable body are 2508 m and 2195 m, respectively. Two layers of filter material are set upstream and downstream of the core wall, respectively. Each thickness of the upstream filter layer is 4 m, while that of the downstream filter layer is 6 m, and the slope ratios of the upstream and downstream filter layers are 1 : 0.2. A transition layer is provided between the upstream and downstream filter layers and the dam shell. The top elevation of the transition layer is 2504 m, the highest width is 10 m, and both the upstream and downstream filter layer slope ratios are 1 : 0.3.

According to the *"Construction Specification for Crushed Earth and Rock Dams" DT/L 5219-2013* and the construction plan of the Shuangjiangkou rockfill dam filling and rolling, a variety of dam materials should be sampled and tested after the completion of filling and rolling before continuing to fill. The test requirement meets the following principles: 8 groups are tested for each filled layer of gravel soil; 2 groups are tested for each filled layer of filter material; 1 group is tested for each filled layer of the transitional rockfill, upstream and downstream; and 2 groups are tested for each layer of each rockfill area.

The maximum design height of the Shuangjiangkou core wall rockfill dam is 315 m. According to the principle of compaction quality inspection, the sampling requirements for various dam materials are shown in Table 3. In the compaction quality inspection of Shuangjiangkou core wall rockfill dam, the total number of sampling inspections exceeded 10000. The traditional water-filling method has a significant error in measuring the volume of the test pit, which can lead to continuous accumulation of measurement errors and even further cause quality changes, leading to a decrease in the overall quality of the dam. High rockfill dams have put forward higher requirements for compaction quality inspection, and traditional inspection methods are gradually unable to meet the requirements of inspection quality and efficiency. Therefore, the research results of this paper apply to the compaction quality inspection of the Shuangjiangkou core wall rockfill dam.

3.2. Method Application

3.2.1. Data Processing. The point cloud data were collected from the sampling test pit during the compaction quality inspection of the Shuangjiangkou core wall rockfill dam material. In order to make the data more general and universal, point cloud data of test pits on four types of dam materials were obtained, including 2 sets of filter material, 5 sets of core wall material, 5 sets of transition rockfill, and 2 sets of rockfill. Figure 18 shows the point cloud data of two sets of test pits for each type of dam material.

In the compaction quality inspection program, the first step is to perform relevant processing on point cloud data, including point cloud segmentation, model reconstruction, spatial coordinate system transformation, and other operations. The point cloud processing results of each stage are extracted, as shown in Figures 19–22.

The results show that the point cloud data processing method proposed in this paper can effectively divide the initial point cloud data collected on the core wall material, filter material, transition material, and rockfill material into dam material surface point cloud data and test pit surface point cloud data, and successfully obtain a test pit closure model using the coordinate plane XOY as the excavation surface of the test pit. In addition, when the point cloud of the dam material surface near the boundary of the test pit is incomplete, the segmentation method in this paper still avoids incorrectly recognizing the point cloud of the test pit surface as the point cloud of the dam material surface and obtains the correct segmentation results.

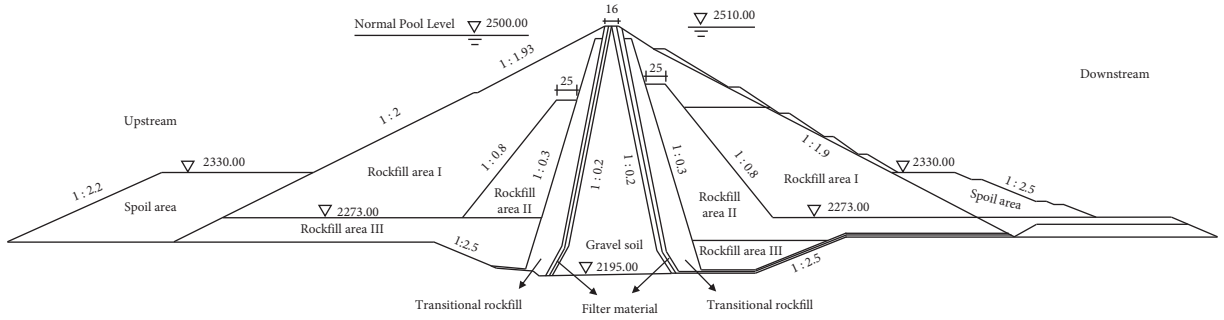

Figure 17: Schematic diagram of filling material zoning for the Shuangjiangkou rockfill dam.

Table 3: Sampling requirements of the Shuangjiangkou rockfill dam for compaction quality testing.

	Maximum particle size (m)	Paving thickness (m)	Test pit diameter (m)/depth (m)	Number of sampling per layer	Total
Gravel soil	0.10	0.30	~0.30/~0.30	6	>6000
Filter material	0.08	0.30	~0.30/~0.30	4	>4000
Transition rockfill	0.30	0.60	~0.90/~0.60	2	>1000
Rockfill	0.80–1.00	1.00	~2.00/~1.00	—	>1000

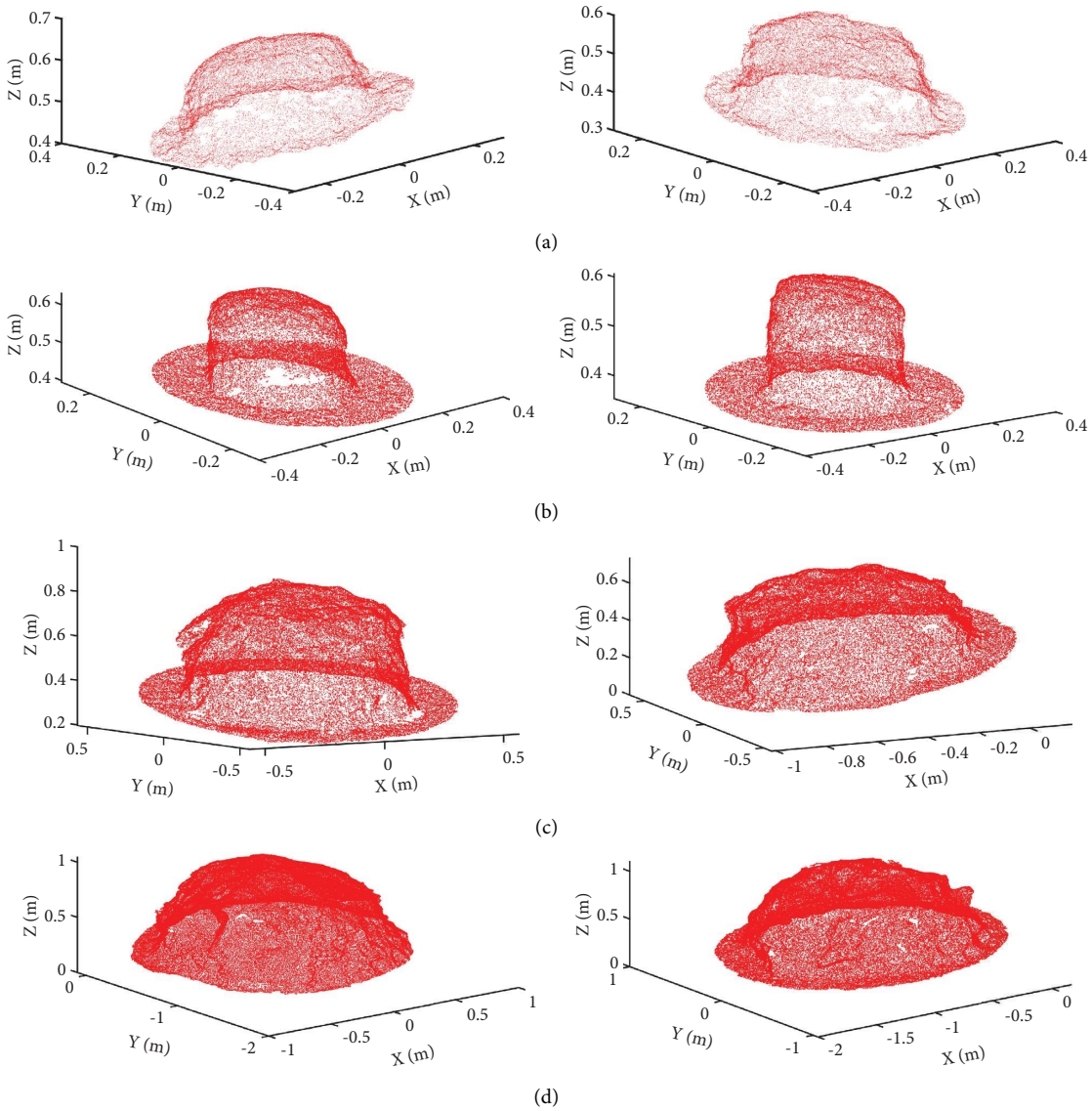

Figure 18: Initial point cloud data. (a) Core wall material. (b) Filter material. (c) Transition rockfill. (d) Rockfill.

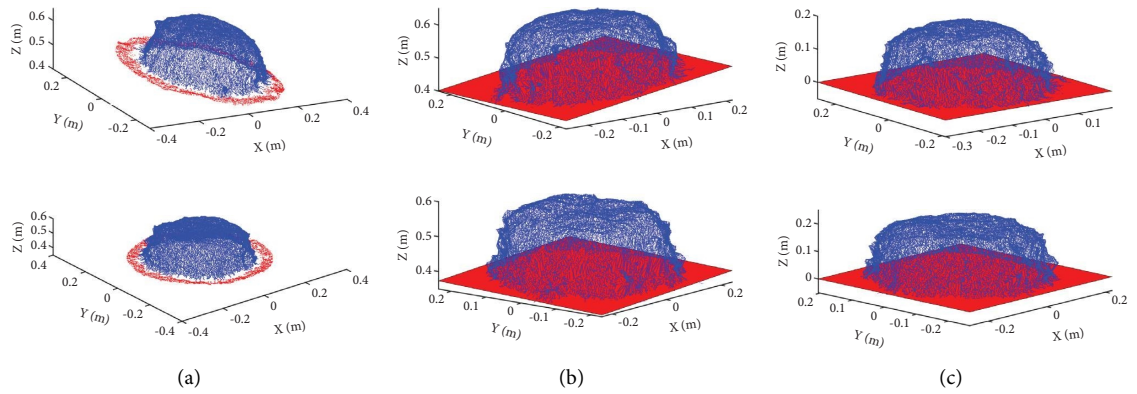

FIGURE 19: Result of point cloud data processing for core wall materials. (a) Point cloud segmentation. (b) Model reconstruction. (c) Spatial coordinate system transformation.

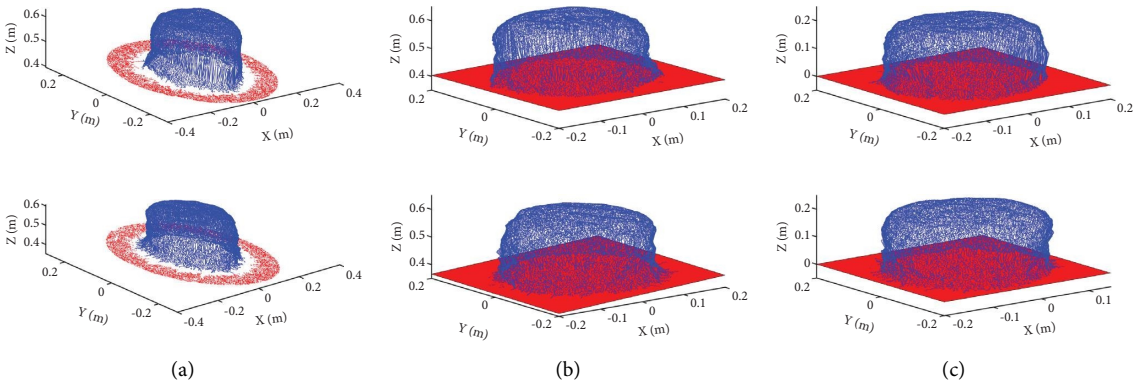

FIGURE 20: Result of point cloud data processing for filter materials. (a) Point cloud segmentation. (b) Model reconstruction. (c) Spatial coordinate system transformation.

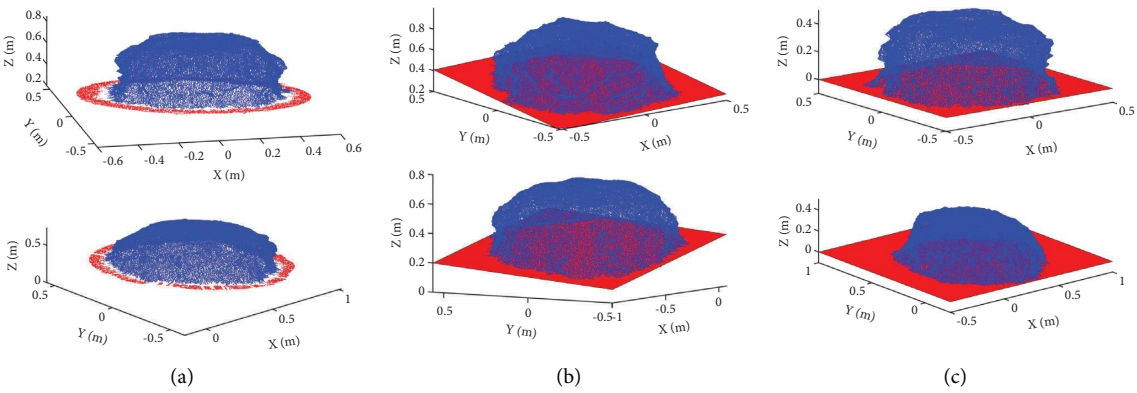

FIGURE 21: Result of point cloud data processing for transition rockfill. (a) Point cloud segmentation. (b) Model reconstruction. (c) Spatial coordinate system transformation.

3.2.2. Calculation of Quality Index. After processing the point cloud data of the test pit, the relevant index for compaction quality inspection is further calculated. According to the Specification for Rolled Earth-rockfill Dam Construction DT/L 5219-2013, compaction control indicators for the core wall are dry density, moisture content, or compaction ratio. The compaction control indexes for the filter material are dry density or relative density. The compaction control index for transition rockfill and rockfill material is porosity. In order to verify the accuracy of the compaction quality inspection method proposed in this paper and compare its advantages with traditional methods, the traditional water-filling method was also used to measure the volume of the test pit. The volume of the test pit measured by the water-filling method is used as the reference value (V_w), while the volume of the test pit measured by this

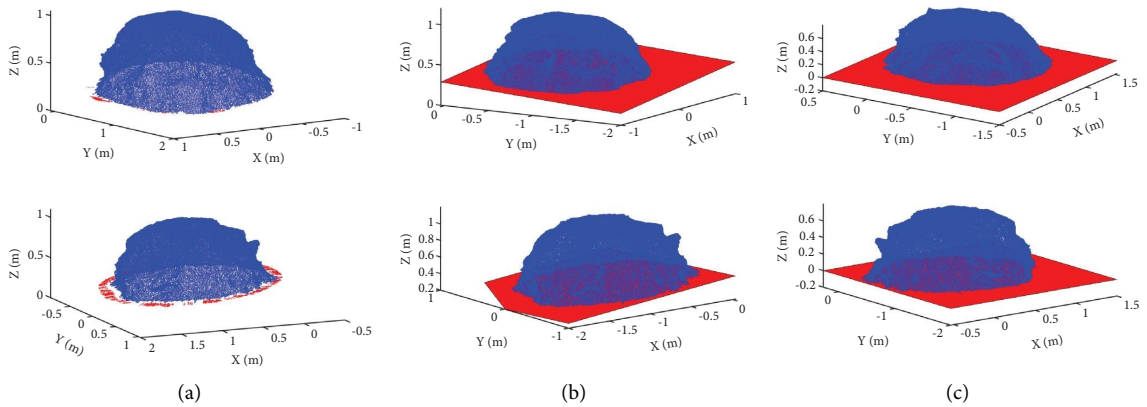

FIGURE 22: Result of point cloud data processing for rockfill. (a) Point cloud segmentation. (b) Model reconstruction. (c) Spatial coordinate system transformation.

method is used as the measurement value (V_s). The relative error between V_w and V_s is used to evaluate the measurement results. The compaction quality inspection results are listed in Table 4, where T_s represents the collection time of point cloud data and T_w represents the irrigation time.

The results show that the measured value V_s of the test pit volume obtained by the method in this paper is close to the reference value V_w measured by the water-filling method, with a maximum relative error of 3.08%, which is relatively small. It can be seen that the method of using the fitting plane of the point cloud on the dam material surface as the excavation surface of the test pit is suitable for quality index detection of various types of dam materials. In terms of measurement efficiency, the collection time of point cloud data is much shorter than the irrigation time, greatly improving measurement efficiency.

Through the analysis of volume errors on different dam materials, it was found that the error of the inverted filter material was the smallest, the error of the core wall material was the largest, and the error of the transition rockfill and rockfill was close. This is because the flatter the dam material surface, the smaller the error of the method in this paper. The more severe the surface roughness of the pit wall, the greater the error of the water-filling method [41]. For the core wall material test pit, due to the slightly lower flatness of the dam material surface and the presence of certain concavities on the pit wall, the measurement value V_s and reference value V_w have the greatest error. For the inverted filter material test pit, due to the high flatness of the dam material surface and the smooth pit wall, the error between the measured value V_s and the reference value V_w is the smallest, which is close to the actual volume of the test pit. The smoothness of the transition material and rockfill material dam material surface is relatively high, but the pit wall is severely uneven, resulting in the reference value V_w always being small. The results show that the measured values V_s in the volume calculation results are greater than the reference value V_w except for the second group of the core wall material, and the error between the measured values and the reference value of the second group of the core wall material is very small, less than 1%. This method is closer to the actual volume of the test pit for the filter material, transition rockfill, and rockfill material measured value V_s. For the core wall material due to its smaller test pit volume and more regular shape, the measurement error is basically negligible with the water-filling method.

In summary, the error between the proposed method and the water-filling method in the results is relatively small. Through the analysis of the reasons for the error, it can be concluded that the quality index test method proposed in this paper has higher accuracy than the water-filling method. At the same time, it avoids the influence of human factors on the measurement results, resulting in higher stability. In addition, the test efficiency has been greatly improved.

3.3. Stability Evaluation. During the test pit point cloud segmenting, the compaction surface point clouds required to fit the plane are determined with $N = 2$ (Figure 11), and their width is related to that of the total scanned dam surface point clouds. However, when collecting the point clouds, the width of the scanned dam surface is different for each scan, resulting in a difference in determining the compaction surface point clouds with $N = 2$. Therefore, it is necessary to verify the effect on the test pit volume measurement results when the fitting plane is performed with different compaction surface point clouds. Different compaction surface point clouds ($N = 6$, 5, 4, 3, 2) are selected, and related volumes of the test pit are calculated, as shown in Table 5. The relative standard deviation (RSD) of the measurement results is used to reflect the effect of selecting different compaction surface point clouds on the volume calculation. The results show that in the compaction quality testing of various types of compacted dam materials, the volume calculation results of selecting different compaction surface point clouds fluctuate very little around their average values, with a maximum RSD of only 0.3859%. Thus, the measurement results do not vary much when selecting different compaction surface point clouds. This result is a powerful index to prove the stability of this method.

Table 4: The results of the index for compaction quality inspection.

		V_s (L)	T_s (s)	V_w (L)	T_w (s)	Relative error (%)	Index
Filter material	1	14.17	~120	14.26	~480	−0.63	Relative density 0.85
	2	14.03		13.90		0.94	Relative density 0.87
Core wall material	1	17.66	~120	17.32	~480	1.96	Compaction ratio 99.1%
	2	20.15		20.34		−0.93	Compaction ratio 99.5%
	3	18.29		17.85		2.46	Compaction ratio 98.6%
	4	15.72		15.25		3.08	Compaction ratio 99.1%
	5	17.16		17.10		0.35	Compaction ratio 99.5%
Transition rockfill	1	199.46	~300	198.82	~1200	0.32	Porosity 20.1%
	2	220.95		218.25		1.24	Porosity 20.9%
	3	224.64		220.08		2.07	Porosity 21.6%
	4	198.91		196.55		1.20	Porosity 20.5%
	5	202.28		198.19		2.06	Porosity 22.0%
Rockfill	1	821.78	~600	805.95	~2000	1.96	Porosity 20.9%
	2	907.85		889.30		2.09	Porosity 21.2%

Table 5: Test pit volumes are calculated by selecting different compaction surface point clouds.

Volume (L)	$N=6$	$N=5$	$N=4$	$N=3$	$N=2$	RSD (%)
Filter material	14.1271	14.1823	14.1833	14.1268	14.1655	0.2001
Core wall material	17.6250	17.5283	17.5156	17.5152	17.6576	0.3859
Transition rockfill	200.4535	200.2329	199.5511	199.4930	199.4607	0.2345
Rockfill	821.4253	821.8257	820.4064	821.0390	821.7822	0.0718

4. Discussion

In the compaction quality inspection of the rockfill dam, the traditional filling-water method is still used on-site (Figure 1(III-2)), but this method has unavoidable defects. First, the pit shape is highly irregular, resulting in the plastic film not being able to adhere to the pit wall, so the water cannot completely fill the test pit. The above reasons produce the result that the pit volume is smaller than the actual volume [41]. In this paper, by extending the scanning equipment into the interior of the test pit, the point cloud data are collected by adjusting the scanning angle and distance in real time, thus obtaining the high-quality point cloud data of the irregular test pit. Second, the plastic film has a certain thickness. In the water-filling method, the thickness of the plastic film is generally 0.1 mm. Chen [13] showed that the volume measurement of the test pit had an error of 2-3% under a 0.1 mm film thickness. 3D laser equipment collects test pit point cloud data directly in a noncontact manner. Third, the human factor in the measurement process is the most difficult variable to control. In the water-filling method, it is judged that the position of twice irrigating is the same by the person, often leading to an unstable measurement result and low reliability. In addition, for the transition rockfill, rockfill material, and other larger diameters of the dam material, the test pit needs to be filled by pouring water back and forth several times, which will inevitably result in a large amount of water being spilled, leading to the error [13, 41]. This paper proposes a volume measurement method using the fitting plane of the compaction surface point clouds as the test pit surface. The site condition that the surface of the pressed dam material is approximately flat provides the basis for the method. Besides, the slicing method accurately divides the pit point clouds into the compaction surface point clouds and the test pit point clouds, while the pit volume was also calculated by selecting different point clouds from the compaction surface to verify the stability of the method, thus ensuring the test accuracy and stability. Finally, the water-filling method has the problem of being time-consuming and labor-intensive but inefficient, especially for volume measurement of large test pits, which requires multiple irrigations and must be reworked once the film breaks. However, the new method requires only one person to complete the data acquisition, and the test result is obtained by importing the collected data into the program written in MATLAB. The test results prove that the method described in this paper is better than the water-filling method in terms of test accuracy, speed, stability, and cost.

The method protest pit closure model using the coordinate plane XOY as the excavation surface of the test pit posed in this paper still has some shortcomings. For example, during the data processing, the point cloud holes were filled in a linear way, which may lead to some local deviations between the test pit point cloud model and the actual test pit. However, most of the test pit point cloud holes are less than 2 cm in diameter, so for the volume calculation of the entire test pit, the effect is minimal and almost

negligible. The advantage of linear filling in this paper is that the hole filling can be done at the same time as the point cloud segmentation, which greatly improves the data processing speed.

5. Conclusion

In order to improve the precision and speed of compaction quality inspection, this paper proposes a method to calculate the volume of the test pit by slicing and segmenting point cloud data based on 3D laser technology. An auxiliary device is developed that allows the handheld scanner's scanning distance and angle to be changed, and its scanning method is also determined to capture high-quality point cloud data. In data processing, it mainly includes two stages. First, the initial point cloud data are accurately divided into compaction surface point clouds and test pit point clouds by the method of segmenting the sorted slicing point clouds. The plane fitted by the compaction surface and test pit point clouds is then registered into a closed model to estimate volume. During volume calculation, the Rodrigues formula and the method of comparing the Z-value of point clouds are used to ensure the calculation's accuracy.

The results of the application in the field show that the relative error between the new method and the traditional water-filling method is 0.14–2.31%, illustrating the accuracy of the new method. However, the new method is better in terms of labor input and work efficiency. The volume is calculated by selecting different areas of the compaction surface, and the maximum relative standard deviation is only 0.3859%, proving the new method's stability. Finally, the error reason for the water-filling method is analyzed, and it is indicated that the method in this paper is closer to the real volume of the test pit in theory.

There are still some key issues that need to be addressed in the future, such as the development of intelligent and rapid excavation machinery for test pits. Currently, detection pits still need to be manually excavated, which is time-consuming and labor-intensive. The future development of rapid and automatic excavation devices for test pits is very important for further improving the efficiency of compaction measurement. Second, the scanning distance of handheld 3D laser scanners is limited, although relevant devices have been preliminarily developed in this paper, and further optimization research is needed to achieve automation and practicality. Third, this paper proposes corresponding algorithms and programs for the volume and compaction quality of the test pit. In the future, a large number of engineering applications, analysis, and optimization are needed, and it is expected that further optimization and promotion of applications can be carried out in the future.

Data Availability

The data used to support the findings of this study are included within the article.

Conflicts of Interest

The authors declare that they have no conflicts of interest.

Authors' Contributions

Q.Y. and Y.W. collected the data and conceived the manuscript; Y.W. and J.H dealt with point cloud data; H.T.L. and Q.Y. provided funding support and ideas; and S.C.Q., Q.Y., and H.T.L. helped to improve the manuscript. All the authors have read and agreed to the published version of the manuscript.

Acknowledgments

This work was supported by the National Key R&D Program of China (2023YFC3008300 and 2023YFC3008305) and Sichuan Provincial International Science and Technology Collaboration & Innovation Project (2022YFH0078). This research was also funded by the National Natural Science Foundation of China (No. 51809188).

References

[1] B. Xue and Z. Sun, "Economics of hydropower energy: a critical assessment," *Energy Sources, Part B: Economics, Planning and Policy*, vol. 13, no. 1, pp. 33–36, 2018.

[2] R. M. Almeida, Q. Shi, J. M. Gomes-Selman et al., "Reducing greenhouse gas emissions of Amazon hydropower with strategic dam planning," *Nature Communications*, vol. 10, no. 1, p. 4281, 2019.

[3] H. Ma and F. Chi, "Major technologies for safe construction of high earth-rockfill dams," *Engineering*, vol. 2, no. 4, pp. 498–509, 2016.

[4] P. Xiao, R. Zhao, D. Li, Z. Zeng, S. Qi, and X. Yang, "As-built inventory and deformation analysis of a high rockfill dam under construction with terrestrial laser scanning," *Sensors*, vol. 22, no. 2, 2022.

[5] J. Zhao, R. Huang, Y. Yang, L. Wang, X. Liu, and Z. Yang, "Study on field relative density test method of blasting rockfill for high rolled rockfill dams," *IOP Conference Series: Earth and Environmental Science*, vol. 638, no. 1, Article ID 012122, 2021.

[6] Z. Ai, G. Ma, G. Zhang, X. Cheng, Q. Zou, and W. Zhou, "The use of shape accel array for deformation monitoring and parameter inversion of a 300 m ultrahigh rockfill dam," *Structural Control and Health Monitoring*, vol. 2023, Article ID 4101604, 18 pages, 2023.

[7] M. Shi, J. Wang, T. Guan, W. Chen, and X. Wang, "Effective compaction power index for real-time compaction quality assessment of coarse-grained geomaterials: proposal and comparative study," *Construction and Building Materials*, vol. 321, Article ID 126375, 2022.

[8] Q. Chen, Y. H. Zou, M. Tang, and C. R. He, "Modelling the construction of a high embankment dam," *KSCE Journal of Civil Engineering*, vol. 18, no. 1, pp. 93–102, 2014.

[9] J. Gong, D. Zou, X. Kong, J. Liu, and K. Chen, "The simulation of high compressive stress and extrusion phenomenon for concrete face slabs in CFRDs under strong seismic loads," *Soil*

Dynamics and Earthquake Engineering, vol. 147, Article ID 106792, 2021.

[10] S. Huang, W. Zhang, and G. Wu, "Research on real-time supervisory system for compaction quality in face rockfill dam engineering," *Journal of Sensors*, vol. 2018, Article ID 6487405, 11 pages, 2018.

[11] F. Wang, Q. Jin, D. Zhong, and B. Wu, "Rock-fill dam construction quality evaluation based on combination model," in *Proceedings of the 2016 5th International Conference on Energy and Environmental Protection (ICEEP 2016)*, New York, NY, USA, December 2016.

[12] S. Li, H. Li, X. Han, Q. Hou, and X. Yang, "Field compaction tests on rockfill dams based on surface settlement method," *Chinese Journal of Geotechnical Engineering*, vol. 40, pp. 127–131, 2018.

[13] Y. Chen, Z. Hu, and H. Xu, "Influence factors and control measures for the density of rockfill by using irrigation method," *Chinese Journal of Geotechnical Engineering*, vol. 39, pp. 177–181, 2017.

[14] D. Hu, Y. Li, X. Yang, X. Liang, K. Zhang, and X. Liang, "Experiment and application of NATM tunnel deformation monitoring based on 3D laser scanning," *Structural Control and Health Monitoring*, vol. 2023, Article ID 3341788, 13 pages, 2023.

[15] R. Maalek and S. Oude Elberink, "Field information modeling (FIM)™: best practices using point clouds," *Remote Sensing*, vol. 13, no. 5, p. 967, 2021.

[16] L. Zheng and Z. Li, "Virtual namesake point multi-source point cloud data fusion based on FPFH feature difference," *Sensors*, vol. 21, no. 16, p. 5441, 2021.

[17] C. Fotsing, P. Hahn, D. Cunningham, and C. Bobda, "Volumetric wall detection in unorganized indoor point clouds using continuous segments in 2D grids," *Automation in Construction*, vol. 141, Article ID 104462, 2022.

[18] T. Meyer, A. Brunn, and U. Stilla, "Change detection for indoor construction progress monitoring based on BIM, point clouds and uncertainties," *Automation in Construction*, vol. 141, Article ID 104442, 2022.

[19] M. Sedek and A. Serwa, "Semi-automatic approach for forming and processing laser sensing data of urban truss," *SVU-International Journal of Engineering Sciences and Applications*, vol. 2, no. 1, pp. 1–8, 2021.

[20] A. Serwa and M. Saleh, "New semi-automatic 3D registration method for terrestrial laser scanning data of bridge structures based on artificial neural networks," *The Egyptian Journal of Remote Sensing and Space Science*, vol. 24, no. 3, pp. 787–798, 2021.

[21] A. Nabil, A. Serwa, and A. E. Mostafa, "Studying the potentiality of using low cost system based on image analysis technique to survey the gravel's size in asphalt mixes," *Engineering Research Journal*, vol. 167, no. 0, pp. 257–274, 2020.

[22] M. Sedek and A. Serwa, "Development of new system for detection of bridges construction defects using terrestrial laser remote sensing technology," *The Egyptian Journal of Remote Sensing and Space Science*, vol. 19, no. 2, pp. 273–283, 2016.

[23] Y. Li, P. Liu, H. Li, and F. Huang, "A comparison method for 3D laser point clouds in displacement change detection for arch dams," *ISPRS International Journal of Geo-Information*, vol. 10, no. 3, p. 184, 2021.

[24] S. Cho, S. Park, G. Cha, and T. Oh, "Development of image processing for crack detection on concrete structures through terrestrial laser scanning associated with the octree structure," *Applied Sciences*, vol. 8, no. 12, p. 2373, 2018.

[25] D. Pagliari, L. Rossi, D. Passoni, L. Pinto, C. De Michele, and F. Avanzi, "Measuring the volume of flushed sediments in a reservoir using multi-temporal images acquired with UAS," *Geomatics, Natural Hazards and Risk*, vol. 8, no. 1, pp. 150–166, 2017.

[26] Y. Huang, S. Hou, H. Ling, and H. Xu, "Trunk volume prediction of individual Populus euphratica trees based on point clouds analysis," *Ecological Indicators*, vol. 95, pp. 964–971, 2018.

[27] M. Kunz, C. Hess, P. Raumonen et al., "Comparison of wood volume estimates of young trees from terrestrial laser scan data," *iForest: Biogeosciences and Forestry*, vol. 10, no. 2, pp. 451–458, 2017.

[28] R. Fang and B. M. Strimbu, "Comparison of stem volume estimates from terrestrial point clouds for mature Douglas-fir (Pseudotsuga menziessi (Mirb.) Franco)," *Information Processing in Agriculture*, vol. 10, no. 3, pp. 334–346, 2023.

[29] M. I. Marzulli, P. Raumonen, R. Greco, M. Persia, and P. Tartarino, "Estimating tree stem diameters and volume from smartphone photogrammetric point clouds," *Forestry: International Journal of Financial Research*, vol. 93, no. 3, pp. 411–429, 2020.

[30] J. Zhao, X. Wang, H. Tian, Y. Lu, C. Guo, and H. Liu, "A fertilizer discharge detection system based on point cloud data and an efficient volume conversion algorithm," *Computers and Electronics in Agriculture*, vol. 185, Article ID 106131, 2021.

[31] Q. Shao, X. Tao, T. Yoshino, Y. J. Zhao, W. T. Yang, and Z. Hang, "Point cloud simplification algorithm based on particle swarm optimization for online measurement of stored bulk grain," *International Journal of Agricultural and Biological Engineering*, vol. 9, 2016.

[32] Z. Cai, C. Jin, J. Xu, and T. Yang, "Measurement of potato volume with laser triangulation and three-dimensional reconstruction," *IEEE Access*, vol. 8, pp. 176565–176574, 2020.

[33] F. Wang, F. Li, V. Mohan, R. Dudley, D. Gu, and R. Bryant, "An unsupervised automatic measurement of wheat spike dimensions in dense 3D point clouds for field application," *Biosystems Engineering*, vol. 223, pp. 103–114, 2022.

[34] J. Guevara, T. Arevalo-Ramirez, F. Yandun, M. Torres-Torriti, and F. A. Cheein, "Point cloud-based estimation of effective payload volume for earthmoving loaders," *Automation in Construction*, vol. 117, Article ID 103207, 2020.

[35] R. Vallejos, F. Yandún, M. A. San Martín, V. Escobar, C. Román, and F. A. Cheein, "Assessing the estimation of trawling catches using LiDAR sensor technology," *Ocean & Coastal Management*, vol. 165, pp. 99–108, 2018.

[36] H. L. Chi, M. K. Kim, K. Z. Liu, J. Thedja, J. Seo, and D. E. Lee, "Rebar inspection integrating augmented reality and laser scanning," *Automation in Construction*, vol. 136, Article ID 104183, 2022.

[37] A. Chéruel and M. B. Ftima, "Unrestrained ASR volumetric expansion for mass concrete structures: review and experimental investigation using 3d laser scanning," *Construction and Building Materials*, vol. 399, Article ID 132565, 2023.

[38] G. Percoco, "Heuristics for direct slicing of point clouds for layered manufacturing," *Advanced Materials Research*, vol. 83-86, pp. 244–249, 2009.

[39] J. Xu, W.-B. Hou, and H. Zhang, "An improved virtual edge approach to slicing of point cloud for additive manufacturing," *Computer-Aided Design and Applications*, vol. 15, no. 3, pp. 330–336, 2017.

[40] S. Yuwen, G. Dongming, J. Zhenyuan, and L. Weijun, "B-spline surface reconstruction and direct slicing from point clouds," *The International Journal of Advanced Manufacturing Technology*, vol. 27, no. 9-10, pp. 918–924, 2006.

[41] H. Wang, J. Gu, and T. Zhang, "Analysis of affecting facors and error control of filling quality detection of rockfilm dam using irrigation method," *Water Resources Planning and Design*, vol. 2020, pp. 84–88, 2020.